

The free path and generation rate of fast-moving electron interacting with dielectric media

M.E. Yeliseiev

Taras Shevchenko Kyiv National University, 64, Volodymyrska str., 01601 Kyiv, Ukraine
E-mail: mykola.eliseev@gmail.com

Abstract. In the framework of macroscopic continuous medium approach, we have studied interaction between a fast-moving charged particle and dielectric or semiconducting media with low energy electrically active excitations. The excitations contribute to frequency dispersion of the media dielectric permittivity. Two types of processes induced by a moving charged particle have been considered: electron-hole generation under interband transitions and excitation of polar optical phonons. For both processes, we calculated and analyzed the time- and space-dependent electric potential generated by the charged particle, polarization of the media, energy losses of the particle and other important constituents of the interaction patterns. Obtained results can contribute to deeper understanding of the charged particle beams interaction with a semiconducting medium, as well as may be useful for versatile applications of charged beams.

Keywords: free path, electron-hole generation, optical phonon, interband transition, electron beam.

<https://doi.org/10.15407/spqeo25.01.010>
PACS 31.15.vj, 71.10.Li, 71.15.Qe, 71.35.-y

Manuscript received 02.09.21; revised version received 10.11.21; accepted for publication 22.03.22; published online 24.03.22.

1. Introduction

The problem of interaction between fast charged particles and dielectric or semiconducting media is of particular interest for both fundamental standpoint and various applications. The fundamental aspects of the problem are related, for example, to the mechanisms of different type excitations in the medium, energy losses of the particles, *etc.* Applications of the problem include scanning electron microscopy using high-quality electron beams [1–4], cathode luminescence effects [5–8], terahertz radiation from plasmon-polaritons excited by electrons [9–12], surface-plasmon resonance sensors [13–16], solid state charge particle detectors [17–19] and others [20–22]. An important application of our results can be found in betavoltaics [23–26]. In this technology, high-energy electrons pass through a dielectric media providing generation of electron-hole pairs, separation of which in *p-n* junctions gives rise to the voltaic effect. Energy cells based on this principle can be used in a number of applications [15–18].

In general, interaction of a charged particle with a media depends on atoms/ions composing the media and its particular structure. However, there exist examples for which this detailed knowledge is not necessary – instead a macroscopic continuous medium approach is applicable. Indeed, the moving charged particle induces time- and space-dependent electrostatic potential. At a distance r

from the particle trajectory, the main contribution to this potential comes with the frequency of the order of

$\omega \approx \frac{v_0}{r}$, where v_0 is the speed of the moving particle.

Thus, electrically active excitations with low frequencies (and energies approximately equal to $\frac{\hbar v_0}{r}$), if they exist, can be produced at macroscopically large distances r ($r \gg a_0$, with a_0 being a lattice constant).

These low energy excitations can be analyzed by using a macroscopic continuum media approach. This approach does not account for the impact of the lattice defects or separate atoms. It can be justified by the fact that we find and check some “characteristic length and frequency scales” in the process of our calculations. The scales are dependent on the speed of the charged particle. Thus, implying a condition that the characteristic scale is considerably higher than the lattice constant, we obtain the lower limit of the particle speed:

$$v_0 \gg a \omega_{gap} = 1.67 \cdot 10^5 \text{ m/s}. \quad (1)$$

It means that the initial energy of the particle needs to be high enough. In this case, the considered charge carrier is not influenced by the individual features of media, which can be treated macroscopically in the frame of frequency-dependent dielectric permittivity. In this work, two models of electrical excitations have been studied.

For interband excitations induced by the fast electrons (*e.g.*, cathode luminescence), we used the permittivity dispersion $\varepsilon(\omega)$ accounting transitions between electron energetic bands in a semiconductor media [12]:

$$\varepsilon' = \varepsilon_0 + \frac{A}{\chi^2} \left(2 - \sqrt{1+\chi} + \sqrt{1-\chi} \theta(1-\chi) \right), \quad (2a)$$

$$\varepsilon'' = \frac{A}{\chi^2} \sqrt{1-\chi} \theta(1-\chi). \quad (2b)$$

Here, ε' is the real part and ε'' – imaginary one of the dielectric permittivity, A – oscillator force, and $\chi = \frac{\hbar\omega}{E_{gap}}$

– dimensionless frequency, E_{gap} – energy band gap, θ – Heaviside step function, ε_0 – material constant.

For consideration of a polar material at the excitation of optical phonons, we consider the permittivity in the form [27]:

$$\varepsilon_{phon} = \chi_\infty \frac{\omega_{lo}^2 - \omega^2 - 2i\gamma\omega}{\omega_{to}^2 - \omega^2 - 2i\gamma\omega}, \quad (3)$$

where χ_∞ is the static permittivity of the media, and ω_{lo} , ω_{to} are the frequencies of the longitudinal and transverse phonons, respectively [12]. The parameter γ is the decay factor. The excitation of the polar medium can be characterized by the induced polarization \mathbf{P} that is related to the dielectric displacement \mathbf{D} and the electric field \mathbf{E} of the moving charge by the formula

$$\vec{D} = \vec{E} + 4\pi\vec{P}. \quad (4)$$

2. Basic assumptions and equations

At first, we consider a particle with a charge q moving with a speed v in a medium with the dispersion law of the dielectric permittivity defined by Eq. (2). The speed v is assumed to be high, but sufficiently smaller than the speed of light (nonrelativistic case), then we neglect magnetic fields around the moving charge particle and use electrostatic equations. In the first approximation the particle speed is considered to be constant (*i.e.*, excited medium does not affect the particle motion), this allows determining the electrical potential, the electric fields and the energy losses of the particle. Then, using the obtained energy losses we can write an approximate differential equation of particle deceleration. From this equation, we determined the dependence of the particle speed on the coordinate along its motion. Because there are no magnetic fields, we use the Maxwell equation for the electric displacement in the differential form. Due to the frequency dispersion of media, we need to use the response convolution function [Помилка! Закладку не визначено.]. By doing that, it becomes possible to link the electric field and the displacement. So, the equations are as follows:

$$\begin{cases} \operatorname{div}(\vec{D}) = 4\pi q \delta(x-vt) \delta(y) \delta(z) \\ \vec{D}(x, y, z, t) = \int_{-\infty}^0 \varepsilon(t-\tau) \vec{E}(x, y, z, t) d\tau \end{cases} \quad (5)$$

In Eq. (5), the charge density of the moving particle of infinitesimal size is written by means of the Dirac delta-function. To make further calculations easier, we have made a Fourier transform on time, and transfer to the Poisson equation for the scalar potential. It is possible to do because $\operatorname{rot} \vec{E} = 0$. So, let us write the electric potential in the form:

$$\Delta\varphi(\omega, \vec{r}) = -\frac{4\pi q}{v\varepsilon(\omega)} e^{+i\omega\frac{x}{v}} \delta(y) \delta(z). \quad (6a)$$

The Fourier image of Eq. (5) can be solved using the Green function, and the general solution for the image of the potential is:

$$\varphi = \iiint_{-\infty}^{+\infty} G(x, \tilde{x}, y, \tilde{y}, z, \tilde{z}) \frac{1}{v} e^{i\omega\frac{x}{v}} \delta(\tilde{y}) \delta(\tilde{z}) d\tilde{x} d\tilde{y} d\tilde{z}. \quad (6b)$$

The boundary conditions for Eq. (5) are that the displacement or the potential decay to zero at infinity, and the Green function $G(x, \tilde{x}, y, \tilde{y}, z, \tilde{z})$ satisfies them.

3. Infinite medium case

3.1. The calculation of the electric potential

We imply that the formula (6b) leads to the following form of the electric potential:

$$\varphi = B \left\{ \begin{aligned} & \int_0^1 \lambda(\chi) \cos(\chi x') K_0\left(\chi \sqrt{y'^2 + z'^2}\right) d\chi + \\ & + \int_1^{+\infty} \mu(\chi) K_0\left(\chi \sqrt{y'^2 + z'^2}\right) d\chi \end{aligned} \right\}. \quad (7a)$$

The following designations are used in Eq. (7a):

$$\lambda(\chi) = \frac{1}{\varepsilon_0 + \frac{A}{\chi^2} \left(2 - \sqrt{1+\chi} + \sqrt{1-\chi} \right)}, \quad (7b)$$

$$\mu(\chi) = \frac{\left(\varepsilon_0 + \frac{A}{\chi^2} \left(2 - \sqrt{1+\chi} \right) \right) \cos(x'\chi) - \frac{A}{\chi^2} \sqrt{\chi-1} \sin(x'\chi)}{\left(\varepsilon_0 + \frac{A}{\chi^2} \left(2 - \sqrt{1+\chi} \right) \right)^2 + \frac{A^2}{\chi^4} (\chi-1)}. \quad (7c)$$

And the dimensionless frequency

$$\chi = \frac{\hbar\omega}{E_{gap}}. \quad (8a)$$

The dimensionless coordinates:

$$x' = \frac{x-vt}{l}, \quad y' = \frac{y}{l}, \quad z' = \frac{z}{l}, \quad r' = \sqrt{y'^2 + z'^2}. \quad (8b)$$

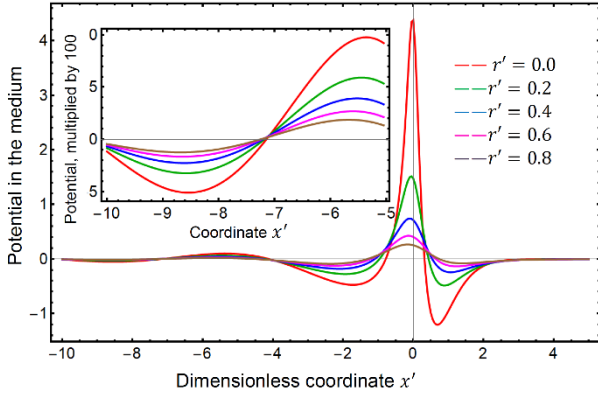


Fig. 1. The dependences of induced potential *versus* longitudinal coordinate x' for various radial distances r' .

The characteristic length and frequency:

$$l = \frac{v}{\omega_{gap}}, \quad \omega_{gap} = \frac{E_{gap}}{\hbar}, \quad (8c)$$

$$B = \frac{q}{\pi v} \frac{E_{gap}}{\hbar}. \quad (8d)$$

The dependence of the induced potential (7) on the coordinates (8b) along the direction of the particle motion is shown in Fig. 1. As one can see from the figure, the potential oscillates for the negative values of the coordinate x' . The inset shows this behavior in more details. The contour map of the potential in coordinates $\{r', x'\}$ is presented in Fig. 2. Since the system is axially-symmetric, the radius-vector lies along the ordinate axis normal to the electron motion. The parameters used in these calculations are shown in Table 1 below.

The obtained electric potential is sign-alternating. It oscillates for the negative values of the longitudinal coordinate and decays to zero in front of the particle. So, if one considers an electron beam in the same medium as a single particle, the property of the potential can lead to some peculiar effects in the beam. Namely, the density of the electrons in the beam can oscillate as well. There will be regions with increased and decreased density. The charged particles can gather in groups due to this effect. Our study cannot prove this mathematically, but there is a high probability that further studies will achieve this result.

Let us consider an electron beam with particles far enough from each other not to disturb their “neighbors” by own electric field. As one can see from Fig. 2, this distance must be not less than ten characteristic lengths

Table 1. The parameters of the media, which are used in our evaluations [28, 29].

Oscillator force A	Material constant ϵ_0	Band gap frequency ω_{gap}
2.6	16	$3 \cdot 10^{15}$ Hz

The material corresponding to these constants is InSb.

(Eq. (8c)). If electrons are distributed denser than this distance, their fields can affect their closest neighbors, and the effect of the density oscillation will occur.

As one can see from Fig. 1, the period of the electric potential oscillations is approximately six characteristic distances. We can say that if two electrons are situated closer than this distance, they influence each other. Thus, some correlations of the density in the electron beam can occur. This means that if electron is located in a cube with the edge longer than the length of six characteristic distances, the density oscillations will not occur. Because in this case, electrons will not influence each other. So, we suggest a way of calculating the current density of a hypothetical beam, in which the electron correlations are still absent:

$$j = ev_0 n. \quad (9a)$$

The concentration n can be estimated as one electron per approximately $10^3 l^3$ volume. So, the current density can be written as follows

$$j = -\frac{e \omega_{gap}^3}{10^3 v_0^2}. \quad (9a)$$

3.2. The energy losses and the coordinate dependence of the particle speed

Let us find the energy losses in the media. To do that, we need to evaluate the field as the gradient of potential (7) and the electric displacement as the response integral. Having the expressions for them, we will be able to find the energy. So, we can write the following formula, being based on Ref. [30, page 306, formula (56.15)]:

$$\frac{d\epsilon}{dx} = -\frac{1}{4\pi} \iiint_V \vec{E} \frac{\partial \vec{D}}{\partial t} dV. \quad (10)$$

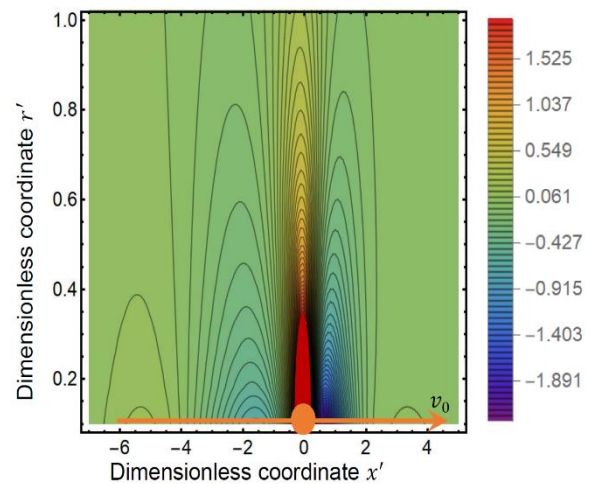


Fig. 2. The contour map of the electric potential defined by Eq. (7). The system is axially-symmetric, so on the ordinate axis the value of the radius-vector normal to the motion of electron, is shown. The orange arrow shows the direction of the electron movement.

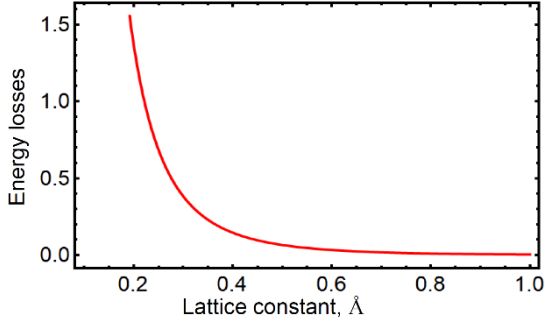


Fig. 3. The dependence of the energy losses per unit length on the cut-off parameter a .

These are the energy losses of the particle in a unit time (or the “power” of the losses). Hence, the particle energy losses per unit length can be written as:

$$\frac{d\varepsilon}{dx} = \int_{-\infty}^{\infty} dt \int_{-\infty}^{+\infty} \rho_{\mathcal{Q}} dy dz, \quad (11)$$

where $\rho_{\mathcal{Q}} = -\frac{1}{4\pi} \frac{\partial \vec{D}}{\partial t} \cdot \vec{E}$. The spatial density of the energy losses can be rewritten as follows:

$$\rho_{\varepsilon}(\omega) = -\frac{1}{4\pi^2} \int_0^{+\infty} \omega |\vec{E}_{\omega}(\omega)|^2 \varepsilon' d\omega = \int_0^{+\infty} \rho_{\varepsilon}(\omega) d\omega. \quad (12)$$

If we substitute the expression for $\vec{E}_{\omega}(\omega)$ into Eq. (12), we obtain the expression for the spatial density of the energy losses per unit frequency interval (*the spectral density*), $\rho_{\varepsilon}(\omega)$:

$$\rho_{\varepsilon}(\omega) = -\frac{1}{4\pi^2} \frac{q^2 \omega^3 \varepsilon'(\omega)}{v_0^4 |\varepsilon(\omega)|^2} \left[K_0^2 \left(r_{\perp} \frac{\omega}{v} \right) + K_1^2 \left(r_{\perp} \frac{\omega}{v} \right) \right]. \quad (13)$$

In the expression (13), $r_{\perp} = \sqrt{y^2 + z^2}$ is the distance from the particle trajectory in the plane perpendicular to this trajectory. In the total energy losses, Eq. (11), the integrand given by Eq. (13) diverges at $r_{\perp} \rightarrow 0$. To get a final value of the integral, we perform the integration starting not from $r_{\perp} = 0$, but from a small distance a . Below, we shall check it for the cut-off parameter a of the order of a few lattice constants, which is natural minimal distance of lattice atoms to the particle, the integral (11) is almost independent of a . It is shown in Fig. 3. We see that the integral term decreases with the increase of a , as a logarithmic function. For actual values of a above a few lattice constants (5...10) Å, the integral changes very little. It proves the validity of the integral cut-off procedure.

We can equate the change of the kinetic energy $T = m \frac{v^2}{2}$ of the particle to the energy loss given by

Eq. (11) and find the derivative of the particle velocity with respect to the coordinate x :

$$\frac{d}{dx} T = mv \frac{dv}{dx} = \frac{dE}{dx}. \quad (14)$$

Here, v is the speed of the particle. Now, the latter can be rewritten as

$$\frac{\Delta\varepsilon}{\Delta x} = -\frac{a^2}{4\pi A} \frac{q^2}{v_0^4 \omega_{gap}^4} I. \quad (15)$$

Where we introduced the following parameter

$$I = \int_1^{\infty} \frac{\chi^5 \sqrt{\chi-1} [K_1(a\chi)K_2(a\chi) - K_0^2(a\chi)]}{\kappa^2 \chi^4 + 2\kappa \chi^2 (2 - \sqrt{1+\chi}) + (2\chi+4) - 4\sqrt{1+\chi}} d\chi \quad (16a)$$

$$\text{with } \kappa = \frac{\varepsilon_0}{A} = 6.153. \quad (16b)$$

The latter value was obtained using the parameters from Table 1. Then, we can solve the differential equation (14) and find the particle speed:

$$v = v_0 \left[1 - \frac{x}{x_{\max}} \right]^{1/6}. \quad (17a)$$

Here, v_0 is the initial speed of the particle. This result shows that the particle decelerates and stops after travelling the distance given by the expression

$$x_{\max} = \frac{2\pi A m \omega_{gap}^4}{3a^2 q^2 I} v_0^6. \quad (17b)$$

All of these transformations and deliberations are possible only if characteristic frequency is significantly higher than the frequency of the interband transition:

$$\frac{v_0}{a} \gg \omega_{gap}, \quad v_0 \gg a \omega_{gap} = 1.67 \cdot 10^5 \text{ m/s}. \quad (17c)$$

So, we can write that $x_{\max} > \frac{2\pi A m a^4 \omega_{gap}^{10}}{3q^2 I}$. The schematic graphical form of the expression (17a) is shown in Fig. 4.

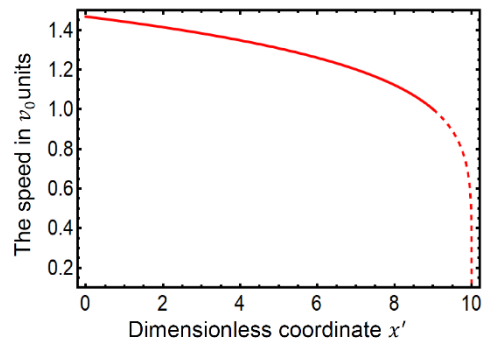


Fig. 4. The dependence of the particle speed on the coordinate x' along its motion.

The result adduced in Fig. 4 shows that a charged particle in the vicinity of a dispersive media slows down and eventually stops. The formula (17a) shows an approximate expression for the maximal distance of the particle motion. The speed is quasi-linear at first, then it rapidly decreases (see the dashed part on the graph). Our calculations can be considered trustworthy for the solid part of the curve, because of the condition (17c) on the value of the speed. The values of the speed represented by the dashed curve decrease rather sharply from the initial value, thus they violate the condition (17c).

3.3. The carrier generation rate evaluation

Let us, knowing the losses density given by expression (13), evaluate the number of the charge carriers generated in a unit space per unit time. To be more precise, we need to know how many interband transitions one electron could cause with the energy it loses in the medium. We will consider such a transition with an energy equal to $\hbar\omega_t$. We can write the following expressions:

$$\frac{d}{dt}n_{gen}(\omega_t)\hbar\omega_t = -\rho_\varepsilon(\omega_t). \quad (18)$$

Here, n_{gen} is the concentration (a number per unit volume) of the interband transitions, ω_t – transition frequency. The equation (18) stems from the energy conservation law. Since the frequency ω_t can have different values in the considered case, we need to integrate Eq. (18) over $\hbar\omega_t$. The result for the generation rate G can be written as follows:

$$G(\tilde{r}_\perp) = \int_{\omega_{gap}}^{\infty} \frac{-\rho_\varepsilon(\omega_t)}{\hbar\omega_t} d\omega_t = \frac{1}{4\pi^2} \frac{q^2}{v_0^4} \int_{\omega_{gap}}^{\infty} \frac{\omega^2 \varepsilon'(\omega)}{\hbar |\varepsilon(\omega)|^2} \left[K_0^2 \left(r_\perp \frac{\omega}{v} \right) + K_1^2 \left(r_\perp \frac{\omega}{v} \right) \right] d\omega. \quad (19a)$$

After conversion of the integral in (19a) to dimensionless parameters, we obtain the following expression:

$$G_{av}(\tilde{r}_\perp) = \int_1^{\infty} G_{av,\chi}(\chi, \tilde{r}_\perp) d\chi. \quad (19b)$$

Here, the generation rate energy density can be written in the following way:

$$G_{av,\chi}(\chi, \tilde{r}_\perp) = \frac{1}{4\pi^2 \hbar} \frac{q^2}{v_0^4 \omega_{gap}^3} \times \frac{\chi^3 \sqrt{\chi-1} \left[K_0^2(\tilde{r}_\perp \chi) + K_1^2(\tilde{r}_\perp \chi) \right]}{\kappa^2 \chi^4 + 2\kappa \chi^2 (2 - \sqrt{1+\chi}) + (2\chi+4) - 4\sqrt{1+\chi}}. \quad (19c)$$

In Eq. (19c) $\chi = \frac{\varepsilon_{pair}}{\varepsilon_{gap}}$, and ε_{pair} is the energy of the generated electron-hole pair. The dimensionless radius-

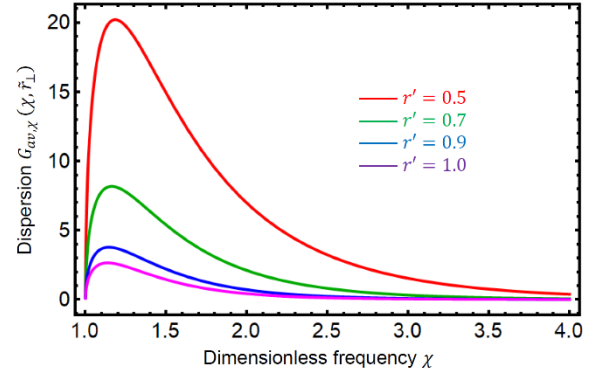


Fig. 5. The dependence of the generation rate dispersion $G_{av,\chi}(\chi, \tilde{r}_\perp)$ on the dimensionless frequency χ for various distances from the charge motion line, which are listed in the legend.

vector absolute value is $\tilde{r}_\perp = \frac{r_\perp}{l}$. To illustrate the analytical expression (19b), a graphical image of the dependence of the generation rate dispersion $G_{av,\chi}(\chi, \tilde{r}_\perp)$ on the dimensionless frequency χ is shown below in Fig. 5.

As one can see from Fig. 5, the dispersion of the generation rate is significantly high for the transition energy close to the band-gap width. For much higher energies, it is insignificant. This can be interpreted as the fact that the moving charge carrier generates only low-energy transitions. So, the macroscopic continuous medium approach is correct, because, as we can see from the figure, the mean energy of the generated transitions is very low. And, naturally, the speed increases with the decrease of the radius-vector absolute value.

Note that the generation rate and the distance of electron penetration for the so-called betavoltaics (which is discussed in Refs [31–33]) is critically important, because of the use of fast electrons with energies around 100 keV.

4. A charged particle near a dielectric with optical phonons/vacuum boundary

4.1. Problem statement

Let us consider a charged particle moving at a fixed distance from the boundary between two media. One of them is a dielectric without dispersion, another is a dielectric with optical phonon dispersion. The speed of the particle is regarded constant. The schematic view of the considered system is shown in Fig. 6.

The permittivities of the media “1” and “2” are:

$$\varepsilon_1 = 1, \quad \varepsilon_2 = \chi_\infty \frac{\omega_{to}^2 - \omega^2 - 2i\gamma\omega}{\omega_{to}^2 - \omega^2 - 2i\gamma\omega}. \quad (20)$$

Let us find the potential, the electric field in both of the media, and the induction. The equations are considered to be the same as (5), with the following boundary conditions:

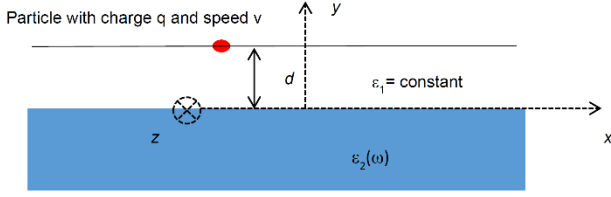


Fig. 6. A particle with a constant charge q and speed v , which moves along the boundary of two dielectrics at the distance d from it.

$$\begin{cases} (D_y^{(1)} - D_y^{(2)})|_{y=0} = 0 \\ (E_x^{(1)} - E_x^{(2)})|_{y=0} = 0 \end{cases} \quad (21)$$

Next, we make the Fourier transform on time and the x coordinate, and a transition to the scalar electrostatic potential, because $\text{rot}(\vec{E}) = 0$. As a result, we obtain the following equations with boundary conditions:

$$\begin{cases} \Delta\varphi(\omega, \vec{r}) = -\frac{4\pi q}{v\varepsilon(\omega)} e^{+i\omega\frac{x}{v}} \delta(y)\delta(z) \\ \Delta\varphi^{(1)}(\omega, \vec{r}) = -\frac{4\pi q}{v\varepsilon_1} e^{+i\omega\frac{x}{v}} \delta(y-d)\delta(z), \quad y > 0 \\ \varepsilon_2\Delta\varphi^{(2)}(\omega, \vec{r}) = 0, \quad y < 0 \\ \varphi^{(1)}|_{y=0} = \varphi^{(2)}|_{y=0} \\ \varepsilon_1 \frac{\partial\varphi^{(1)}}{\partial y}|_{y=0} = \varepsilon_2 \frac{\partial\varphi^{(2)}}{\partial y}|_{y=0} \end{cases} \quad (22)$$

4.2. The electric potential and the field

The solution of Eqs. (22) was found by means of the Green function and has the form:

$$\varphi_1 = \frac{2q}{\pi d} \left\{ \int_0^{+\infty} \cos(\tilde{\omega}x') [K_0(\tilde{\omega}\tilde{B}_-) + K_0(\tilde{\omega}\tilde{B}_+)] d\tilde{\omega} + \int_0^{+\infty} d\tilde{\omega} \left[-2 \left(\cos(\tilde{\omega}x')\tau(\tilde{\omega}) + \sin(\tilde{\omega}x')\sigma(\tilde{\omega}) \right) K_0(\tilde{\omega}\tilde{B}_+) \right] d\tilde{\omega} \right\}. \quad (23)$$

Eq. (23) is written for $y > 0$, in the upper half-space. In the lower half-space (for $y < 0$), the potential has the form:

$$\varphi_2 = \frac{4q}{\pi d} \int_0^{+\infty} \left(\cos(\tilde{\omega}x') - \left\{ \begin{array}{l} \cos(\tilde{\omega}x')\tau(\tilde{\omega}) + \\ + \sin(\tilde{\omega}x')\sigma(\tilde{\omega}) \end{array} \right\} \right) K_0(\tilde{\omega}\tilde{B}_-) d\tilde{\omega}. \quad (24)$$

In Eqs (23) and (24), the following dimensionless factors were used:

Table 2. The values of dimensionless parameters, which are used in our calculations.

$\tilde{\gamma}$	$\tilde{\omega}_{lo}$	$\tilde{\omega}_{to}$	d	χ_∞
0.01	1.2	1	10^{-4}	2.56

Note. The material corresponding to these constants is GaAs.

$$\tau(\tilde{\omega}) = \frac{\varphi_\infty \left((\tilde{\omega}_{lo}^2 - \tilde{\omega}^2) + 4(\tilde{\gamma}\tilde{\omega})^2 \right) + \left((\tilde{\omega}_{lo}^2 - \tilde{\omega}^2) (\tilde{\omega}_{to}^2 - \tilde{\omega}^2) + 4(\tilde{\gamma}\tilde{\omega})^2 \right)}{\left[(\tilde{\omega}_{to}^2 - \tilde{\omega}^2) + \chi_\infty (\tilde{\omega}_{lo}^2 - \tilde{\omega}^2) \right]^2 + 4\tilde{\gamma}^2 \tilde{\omega}^2 (1 + \chi_\infty)^2}, \quad (25a)$$

$$\sigma(\tilde{\omega}) = \frac{\chi_\infty 2\tilde{\gamma}\tilde{\omega} (\tilde{\omega}_{to}^2 - \tilde{\omega}_{lo}^2)}{\left[(\tilde{\omega}_{to}^2 - \tilde{\omega}^2) + \chi_\infty (\tilde{\omega}_{lo}^2 - \tilde{\omega}^2) \right]^2 + 4\tilde{\gamma}^2 \tilde{\omega}^2 (1 + \chi_\infty)^2}. \quad (25b)$$

In Eqs (23)–(25), the following dimensionless parameters were introduced:

$$\tilde{\omega}_{to} = \frac{\omega_{to}}{\omega_v}, \quad \tilde{\omega}_{lo} = \frac{\omega_{lo}}{\omega_v}, \quad \tilde{\gamma} = \frac{\gamma}{\omega_v}, \quad (26a)$$

$$\tilde{B}_\pm = \sqrt{(y' \pm 1)^2 + (z')^2}, \quad (26b)$$

$$x' = \frac{x - vt}{d}, \quad y' = \frac{y}{d}, \quad z' = \frac{z}{d}, \quad (26c)$$

$$\tilde{\omega} = \frac{\omega}{v} d, \quad \omega_v = \frac{v}{d}. \quad (26d)$$

The coordinate dependences of the potential represented by Eqs. (23) and (24) are shown in Fig. 7. The curves were plotted for the parameters listed in Table 2.

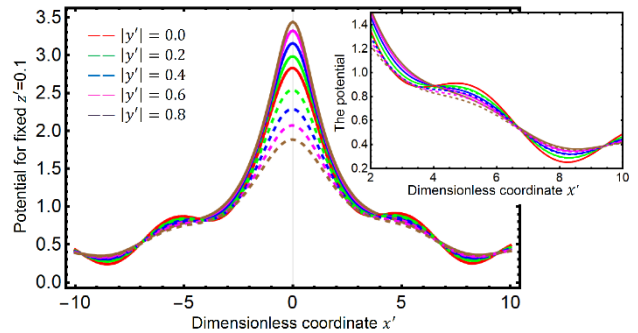


Fig. 7. The dependence of the electrostatic potential on the dimensionless coordinate x' for fixed z' and different y' (different solid and dashed curves). The solid curves correspond to the upper half-space, the dashed curves – to the lower one of the system. The inset shows oscillations of the potential in more details.

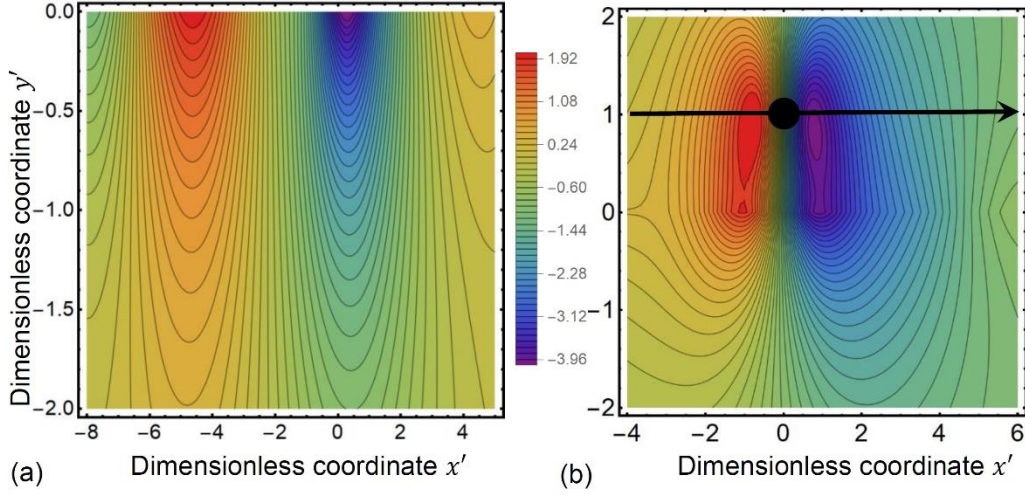


Fig. 8. (a) The space distribution of x -component for the polarization in the dispersive media (28a). (b) The space distribution of the electric field. The black arrow shows the trajectory of the charged particle, the point – its position.

The electric potential oscillates for the positive values of the dimensionless coordinate, as it is shown in the inset of Fig. 7. For the negative values, it oscillates as well. So, the changes of density in the electron beam will occur in this case as well. These oscillations occur for molecules as well, as it is shown in [34].

From the expressions (23) and (24), one can obtain the formulas for the electric field and the polarization in the medium. They are shown below:

$$E_x = \frac{4}{\pi} \frac{q}{d^2} \frac{\chi_\infty}{\epsilon_1} \times \int_0^{+\infty} \tilde{\omega} \begin{bmatrix} -\frac{2}{\epsilon_1} \sin(\tilde{\omega}x') - \\ -\sin(\tilde{\omega}x')\tau(\tilde{\omega}) + \cos(\tilde{\omega}x')\sigma(\tilde{\omega}) \end{bmatrix} K_0(\tilde{\omega}\tilde{B}_-) d\tilde{\omega}. \quad (27a)$$

The x -component of polarization can be written as follows:

$$P_{1x} = q / (\pi^\uparrow 2d^\uparrow 2) x_{\downarrow}^\infty / \epsilon_{\downarrow 1} \int_{\downarrow} 0^\uparrow (+^\infty) \equiv \tilde{\omega} \left\{ \begin{array}{l} \left[\epsilon^{\uparrow'}(\tilde{\omega}) - 1 \right] \left\{ \begin{array}{l} -(2)/\epsilon_{\downarrow 1} \sin(\tilde{\omega}x^{\uparrow'}) - \\ -\sin(\tilde{\omega}x^{\uparrow'})\tau(\tilde{\omega}) + \\ + \cos(\tilde{\omega}x^{\uparrow'})\sigma(\tilde{\omega}) \end{array} \right\} - \\ -\epsilon^{\uparrow''}(\tilde{\omega}) \left\{ \begin{array}{l} (2)/\epsilon_{\downarrow 1} \cos(\tilde{\omega}x^{\uparrow'}) + \\ + \sin(\tilde{\omega}x^{\uparrow'})\sigma(\tilde{\omega}) + \\ + \cos(\tilde{\omega}x^{\uparrow'})\tau(\tilde{\omega}) \end{array} \right\} \end{array} \right\} K_{\downarrow} 0. \quad (28)$$

Here, the imaginary $\epsilon''(\tilde{\omega})$ and the real $\epsilon'(\tilde{\omega})$ parts of the permittivity are derived from Eq. (3). Let us analyze a contour plot of the longitudinal (to the motion of the particle) component of the polarization given by Eq. (28),

and the field defined by Eq. (27). They are shown in Figs 8a and 8b, respectively.

As one can see, electron induces two regions with a significant value of the polarization – one five characteristic distances behind it, and one right in front of it. The field has a similar structure – two regions with significant in value and opposite in sign x -components, one two characteristic distances in front, other two of them behind. If we consider an electron beam in these conditions, we will find that the minimal critical concentration corresponding to the density correlations is equal to $\frac{1}{5^3 d^3}$.

5. Conclusions

In this work, we have considered interaction of a fast-moving charged particle with low-energy electrically active excitations of a dielectric/semiconducting medium. The long-range character of the potential induced by the charged particle facilitates analysis of the low-energy excitations by applying the macroscopic description of dielectric/semiconducting medium. This macroscopic description can be based on characterization of the medium by a dielectric permittivity. Frequency dependence of the dielectric permittivity represents low-energy and electrically active excitations of analyzed medium.

Two particular types of the low-energy excitations have been studied: (i) interband excitations in a semiconductor, (ii) optical phonon excitations in a polar dielectric. Then, we have considered a charged particle moving through an infinite medium, and one moving near the boundary of two dielectric media. We found that for every excitation type and geometry the electric potential induced by the particle, as well as the medium polarization, oscillates with the coordinate along the particle trajectory. Excitations of the medium give rise to energy losses of the moving particle and its deceleration. We have found the approximate coordinate dependence of the particle speed and its path length. We have determined

the spatial patterns of the induced potential, generation rate of the electron-hole pairs under interband excitation and polarization of polar medium.

For the excitation type (i), we have found an analytical formula for the spectral density of the generation rate for electron-hole pairs induced by the fast-moving charged particle. We have proved that the spectral density has significant amplitude only for the frequencies close to the bandgap and rapidly increases in the vicinity of the charge trajectory.

For the excitation type (ii), we found that the moving charged particle creates complex patterns of the electric field and polarization: two regions attendant the particle have significant amplitudes of the field and the polarization, signs of the field and the polarization are opposite in these regions. The moving patterns of the polarization induce complex lattice vibrations in the particle trace.

We suggest that the obtained results can contribute to deeper understanding of physics of interaction between moving charged particles and dielectric/semiconducting media, as well as may be useful for numerous devices and technologies using charged beam-medium interaction [11, 13].

Acknowledgements

I express the deepest gratitude to my scientific supervisor Prof. Dr V.A. Kochelap for the problem statement, guidance, support with analyzing the results and permanent stimulating discussions.

References

- de Abajo F.J.G. Optical excitations in electron microscopy. *Rev. Mod. Phys.* 2010. **82**. P. 209–275. <https://doi.org/10.1103/RevModPhys.82.209>.
- Bashevoy M.V., Jonsson F., Krasavin A.V. *et al.* Generation of traveling surface plasmon waves by free – electron impact. *Nano Lett.* 2006. **6**. P. 1113–1115. <https://doi.org/10.1021/nl060941v>.
- Cai W., Sainidou R., Xu J., Polman A., and de Abajo F.J.G. Efficient generation of propagating plasmons by electron beams. *Nano Lett.* 2009. **9**. P. 1176–1181. <https://doi.org/10.1021/nl803825n>.
- Milton K.A., Li Y., Guo X., Kennedy G. Electrodynamic friction of a charged particle passing a conducting plate. *Phys. Rev. Res.* 2020. **2**. P. 023114. <https://doi.org/10.1103/PhysRevResearch.2.023114>.
- Fano U. A theory on cathode luminescence. *Phys. Rev.* 1940. **58**. P. 544. <https://doi.org/10.1103/PhysRev.58.544>.
- Sugita A., Kamiya M., Morita C. *et al.* Nanometric light spots of cathode luminescence in $Y_2O_3:Eu^{3+}$ phosphor thin films excited by focused electron beams as ultra-small illumination source for high-resolution optical microscope. *Opt. Mater. Exp.* 2014. **4**. P. 155–161. <https://doi.org/10.1364/OME.4.000155>.
- Zhan J., Mu H., Zhang G., Huang X., Shao X., and Deng J. Cathode-like luminescence from vacuum-dielectric interface induced by self-stabilizing secondary electron emission. *Appl. Phys. Lett.* 2012. **101**. P. 041604. <https://doi.org/10.1063/1.4738999>.
- Neubauer, A., Yochelis S., Popov I. *et al.* Local cathode luminescence resonant peak in hybrid organic nanocrystal systems. *J. Phys. Chem. C.* 2012. **116**. P. 15641–15645. <https://doi.org/10.1063/1.4738999>.
- Liu S., Zhang P., Liu W. *et al.* Surface polariton Cherenkov light radiation source. *Phys. Rev. Lett.* 2012. **109**. P. 153902. <https://doi.org/10.1103/PhysRevLett.109.153902>.
- Liu S., Zhang C., Hu M. *et al.* Coherent and tunable terahertz radiation from graphene surface plasmon polaritons excited by an electron beam. *Appl. Phys. Lett.* 2014. **104**. P. 201104. <https://doi.org/10.1063/1.4879017>.
- Gong S., Hu M., Zhong R. *et al.* Electron beam excitation of surface plasmon polaritons. *Opt. Exp.* 2014. **22**. P. 19252–19261. <https://doi.org/10.1364/OE.22.019252>.
- Li R.K., To H., Andonian G. *et al.* Surface-plasmon resonance-enhanced multiphoton emission of high-brightness electron beams from a nanostructured copper cathode. *Appl. Phys. Lett.* 2013. **110**. P. 074801. <https://doi.org/10.1103/PhysRevLett.110.074801>.
- Homola J., Yee S.S., and Gauglitz G. Surface plasmon resonance sensors: review. *Sens. Actuators B Chem.* 1999. **54**. P. 3–15. [https://doi.org/10.1016/S0925-4005\(98\)00321-9](https://doi.org/10.1016/S0925-4005(98)00321-9).
- Davidovich M.V. Amplification of optical and THz surface plasmon-polaritons by electron beams. *Saratov Fall Meeting 2018: Laser Physics, Photonic Technologies, and Molecular Modeling.* 2018. **11066**. P. 1106614.
- Durham D.B., Pierce C.M., Riminucci F. *et al.* Characterizing plasmon-enhanced photoemitters for bright ultrafast electron beams. *Plasmonics: Design, Materials, Fabrication, Characterization, and Applications XIX, International Society for Optics and Photonics.* 2021. **11797**. P. 117972D. <https://doi.org/10.1117/12.2597708>.
- de Abajov G., Javierb F., and Di Giulio V. Optical excitations with electron beams: Challenges and opportunities. *ACS Photonics.* 2021. **8**. P. 945–974. <https://doi.org/10.1021/acsp Photonics.0c01950>.
- Knoll G.F. *Radiation Detection and Measurement* (3rd ed.). Wiley, 1999.
- Durrani S.A., and Bull R.K. *Solid State Nuclear Track Detection: Principles, Methods and Applications.* **111**. Elsevier, 2013.
- Cenna F., Cartiglia N., Friedl M. *et al.* Weightfield2: A fast simulator for silicon and diamond solid state detector. *Nuclear Instruments and Methods in Physics Research Section A: Accelerators, Spectrometers, Detectors and Associated Equipment.* 2015. **796**. P. 149–153. <https://doi.org/10.1016/j.nima.2015.04.015>.
- Boyer T.H. Penetration of the electric and magnetic velocity fields of a nonrelativistic point charge into a conducting plane. *Phys. Rev. A.* 1974. **9**. P. 68–82. <https://doi.org/10.1103/PhysRevA.9.68>.

21. Bashevoy M.V., Jonsson F., Macdonald K.F. *et al.* Hyperspectral imaging of plasmonic nanostructures with nanoscale resolution. *Opt. Exp.* 2007. **15**. P. 11313–11320. <https://doi.org/10.1364/OE.15.011313>.
22. Kyrychenko O.L. On the influence of the density of laser beam energy on the sensitivity of explosive substances to laser radiation. *Scientific Bulletin of National Mining University.* 2018. **6**.
23. Krasnov A.A. and Legotin S.A. Advances in the development of betavoltaic power sources (A review). *Instruments and Experimental Techniques.* 2020. **63**, No 4. P. 437–452. <https://doi.org/10.1134/S0020441220040156>.
24. Olsen L.C. Review of betavoltaic energy conversion. *NASA Conf. Publ.* 1993. P. 256–256.
25. Maximenko S.I., Moore J.E., Affouda C.A., and Jenkins P.P. Optimal semiconductors for 3 H and 63 Ni betavoltaics. *Sci. Repts.* 2019. **9**. P. 1–8. <https://doi.org/10.1038/s41598-019-47371-6>.
26. Heuser T., Braun M., McIntyre P., and Senesky D.G. Electron beam irradiation of gallium nitride-on-silicon betavoltaics fabricated with a triple mesa etch. *J. Appl. Phys.* 2021. **130**, No 17. P. 174503. <https://doi.org/10.1063/5.0069602>.
27. Anselm A.I. *Introduction to Semiconductor Theory: A Study Guide.* St.-Petersburg: Lan, 2017.
28. Lyaschuck Yu.M., Koroteev V.V. Plasmon-enhanced infrared absorption in a thin InSb layer. *Lashkaryov readings*, 2019. V. Lashkaryov Institute of Semiconductor Physics, NAS of Ukraine.
29. Degheidy A.R., Elkenany E.B., Madkour M.A.K., Abuali A.M. Temperature dependence of phonons and related crystal properties in InAs, InP and InSb zinc-blende binary compounds. *Computational Condensed Matter.* 2018. **16**. P. e00308. <https://doi.org/10.1016/j.cocom.2018>.
30. Landau L.D., Lifshitz E.M., Pitaevskii L.P. *Electrodynamics of Continuous Media.* Second Edition. Butterworth-Heinemann, 1984.
31. Guo H. and Lal A. Nanopower betavoltaic micro-batteries. *TRANSDUCERS'03. 12th International Conference on Solid-State Sensors, Actuators and Microsystems. Digest of Technical Papers* (Cat. No. 03TH8664). 2003. **1**. P. 36–39. <https://doi.org/10.1109/SENSOR.2003.1215247>.
32. Yakimov E.B. Prediction of betavoltaic battery output parameters based on SEM measurements and Monte Carlo simulation. *Applied Radiation and Isotopes.* 2016. **112**. P. 98–102. <https://doi.org/10.1016/j.apradiso.2016.03.023>.
33. Thomas C., Portnoff S., and Spencer M.G. High efficiency 4H-SiC betavoltaic power sources using tritium radioisotopes. *Appl. Phys. Lett.* 2016. **108**. P. 013505. <https://doi.org/10.1063/1.4939203>.
34. Tomassone M.S. and Widom A. Electronic friction forces on molecules moving near metals. *Phys. Rev. B.* 1997. **56**. P. 4938–4943. <https://doi.org/10.1103/PhysRevB.56.4938>.

Author and CV



Mykola E. Yelisieiev, born in 2000, defended his bachelor diploma in Theoretical Physics in 2021 at the Taras Shevchenko Kyiv National University. Now he is obtaining a Master's degree in the same university. The area of his scientific interests includes semiconductor physics, quantum mechanics, physics of non-linear processes, as well as the analysis, diagnostics, modeling and forecasting of physical processes in different objects. <http://orcid.org/0000-0001-5129-7113>

Вільний пробіг та темп генерації швидкого електрона, що взаємодіє з діелектричним середовищем

М.Є. Єліссєв

Анотація. У рамках підходу макроскопічного неперервного середовища досліджено взаємодію між швидкою зарядженою частинкою та діелектричним або напівпровідниковим середовищем з низькоенергетичними електронно-активними збудженнями. Ці збудження є причиною частотної дисперсії діелектричної проникності середовища. Розглянуто два типи процесів, викликаних рухомою зарядженою частинкою: генерація електронно-діркових пар при міжзонних переходах та збудження поляричних оптичних фононів. Для обох процесів ми розрахували та проаналізували залежність від часу та простору електричного потенціалу, який генерує заряджена частинка, поляризацію середовища, втрати енергії частинкою та інші важливі параметри моделей взаємодії. Отримані результати можуть сприяти глибшому розумінню взаємодії пучків заряджених частинок з напівпровідниковим середовищем, а також можуть бути корисними для різноманітних практичних застосувань заряджених пучків.

Ключові слова: шлях вільного пробігу, генерація електронно-діркових пар, оптичні фонони, міжзонні переходи, електронні пучки.